AIAA 2002-4408

Experimental Hypersonic Aerodynamic Characteristics of the 2001 Mars Surveyor Precision Lander with Flap

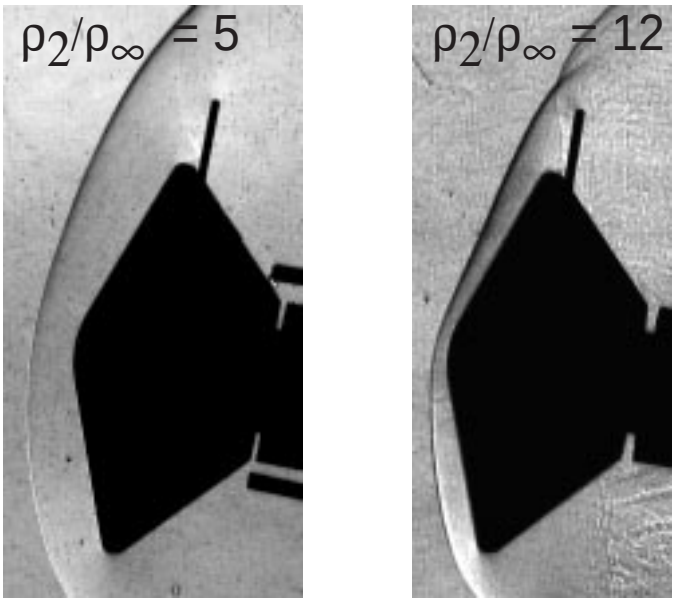

Thomas J. Horvath,
Tod F. O'Connell, F. McNeil Cheatwood,
Ramadas K. Prabhu, and Stephen J. Alter

NASA Langley Research Center
Hampton, Virginia

AIAA Atmospheric Flight Mechanics Conference and Exhibit
August 5-8, 2002 / Monterey, CA

Experimental Hypersonic Aerodynamic Characteristics of the Mars Surveyor 2001 Precision Lander with Flap

Thomas J. Horvath*, Tod F. O'Connell⊕, F. McNeil Cheatwood/·, Ramadas K. Prabhu†
and
Stephen J. Alter*·
NASA Langley Research Center

Abstract

Aerodynamic wind-tunnel screening tests were conducted on a 0.029 scale model of a proposed Mars Surveyor 2001 Precision Lander (70 deg half angle spherically blunted cone with a conical afterbody). The primary experimental objective was to determine the effectiveness of a single flap to trim the vehicle at incidence during a lifting hypersonic planetary entry. The laminar force and moment data, presented in the form of coefficients, and shock patterns from schlieren photography were obtained in the NASA Langley Aerothermodynamic Laboratory for post-normal shock Reynolds numbers (based on forebody diameter) ranging from 2,637 to 92,350, angles of attack ranging from 0 up to 23 degrees at 0 and 2 degree sideslip, and normal-shock density ratios of 5 and 12. Based upon the proposed entry trajectory of the 2001 Lander, the blunt body heavy gas tests in CF_4 simulate a Mach number of approximately 12 based upon a normal shock density ratio of 12 in flight at Mars. The results from this experimental study suggest that when traditional means of providing aerodynamic trim for this class of planetary entry vehicle are not possible (e.g. offset c.g.), a single flap can provide similar aerodynamic performance. An assessment of blunt body aerodynamic effects attributed to a real gas were obtained by synergistic testing in Mach 6 ideal-air at a comparable Reynolds number. From an aerodynamic perspective, an appropriately sized flap was found to provide sufficient trim capability at the desired L/D for precision landing. Inviscid hypersonic flow computations using an unstructured grid were made to provide a quick assessment of the Lander aerodynamics. Navier-Stokes computational predictions were found to be in very good agreement with experimental measurement.

Nomenclature

b_{REF}	reference span of model (3-in)
D	model base diameter (3-in)
L_{REF}	reference length (3-in)
M	Mach number
P	pressure (psi)
r	radius (in)
Re	Reynolds number
S_{REF}	model base reference area (in^2)
T	temperature (¡R)
α	angle of attack (deg)
C_A	axial-force coeff., axial force/$q_\infty S_{REF}$
C_l	rolling-moment coeff., rolling-moment/$q_\infty S_{REF} b_{REF}$
C_m	pitching-moment coeff., pitching-moment/$q_\infty S_{REF} L_{REF}$
C_N	normal-force coeff., Normal force/$q_\infty S_{REF}$
$C_{l,\beta}$	$\Delta C_l/\Delta\beta$, (per degree)
$C_{n,\beta}$	$\Delta C_n/\Delta\beta$, (per degree)
$C_{Y,\beta}$	$\Delta C_Y/\Delta\beta$, (per degree)
L/D	lift to drag ratio
γ	ratio of specific heats
q	dynamic pressure (psi)
ρ	density (lbm/in^3)
θ	angle (deg)
$X_{c.g.}$	c.g. location

Subscripts

β	sideslip angle, (degree)
∞	free-stream conditions
n	model nose
s	surface quantity, support sting
sh	Forebody shoulder
t, 1	reservoir conditions
2	stagnation conditions behind normal shock
w	wall

Introduction

The next generation of Mars landers is being developed by NASA to provide a precision landing

* Aerothermodynamics Branch, NASA Langley Research Center, Hampton, VA.
/ Space Access & Exploration Program Office, NASA Langley Research Center, Hampton, VA.
† Lockheed Martin Engineering & Sciences Co., Hampton, VA.
⊕ Cooperative education student, NASA Langley Research Center, Hampton, VA.
· Senior member, AIAA

capability to within 10 kilometers of the targeted site[1]. This order of magnitude improvement in the accuracy associated with the targeted landing area will potentially enhance hazardous avoidance capability and allow geologically exciting (e.g. ice deposits recently detected beneath the surface of Mars by the orbiting Mars Odyssey spacecraft) or difficult to reach sites to be exploited by unmanned rovers for their scientific value. The demonstration of a precision landing would also represent a technology milestone towards the human exploration of Mars, where crewed expeditions will likely require advanced placement of cargo carriers and habitat modules within several hundred meters of each other.

The Mars Surveyor 2001 Precision Lander[2] (MSPL) was originally part of NASA's ten year Mars Surveyor Program that was initiated in 1994. A precision landing demonstration by the lander, was to have been accomplished through the use of advanced approach navigation techniques coupled with an actively controlled descent into the planetary atmosphere via a vehicle with a moderate Lift-to-Drag capability. As the result of a restructured[3-5] strategy for the exploration of Mars, the planned precision landing demonstration by a lander was dropped from the 2001 mission objectives. Under the present exploration plan, a 2009 opportunity for a precision landing demonstration exists. The entry vehicle for this potential mission is referred to as a Smart Lander[6].

Had the 2001 lander mission been attempted, it would have represented the first autonomously directed entry into Mars by a *lifting* vehicle using an atmospheric guidance algorithm for Mars[7-10]. In contrast to the non-lifting ballistic entries flown by Pathfinder and the Mars Polar Lander and the lifting entries flown by the Viking Landers[11], the initial entry strategy for the 2001 Lander called for directional control of the entry vehicle lift vector through bank angle modulation. Control of the lift vector was to be provided by reaction control jets. To expedite lander construction and minimize cost, the baseline configuration for the 2001 lander was leveraged from Pathfinder and the Mars Polar Lander designs which consisted of a Viking heritage 70-deg spherically blunted cone with a conic afterbody.

Traditionally, such blunt axisymmetric shapes can produce lift by flying at incidence and are aerodynamically trimmed via a center of gravity offset. Because Pathfinder and the Mars Polar lander flew ballistic entries, these flight vehicles did not possess a nominal c.g. offset. Constrained by these previous designs (expedite lander construction/minimize tooling costs), structural and weight constraints of the proposed 2001 lander (which was to fly a *lifting* trajectory) did not permit the radial c.g. offset required for aerodynamic trim (at the desired L/D) that would normally be achieved through payload packaging trades or ballast mass. This required that alternative methods to provide aerodynamic trim be examined[2].

The present paper details an investigation designed to assess the aerodynamic feasibility of one such proposal; a single body flap to trim the lander at angle of attack during hypersonic planetary entry. An inviscid flow solver was used to rapidly evaluate several flaps with the potential to provide sufficient trim capability to meet mission objectives. Experimental force and moment measurements are then compared to Navier—Stokes prediction.

An early Smart Lander concept using a flap to provide aerodynamic trim is shown in Fig. 1. Historically, the concept of a flap to provide aerodynamic trim on similar axisymmetric blunt capsule shapes can be found as early as 1961 and are reported in Ref. 12. As an alternative method to provide aerodynamic trim for the 2001 lander, the viability of the flap would be determined by its ability to provide similar or better aerodynamic performance across the Mach number range relative to that achieved with an offset c.g. For future missions requiring precision landing (where constraints for an offset c.g. are more relaxed) a flap may still serve as an attractive means for providing aerodynamic trim.

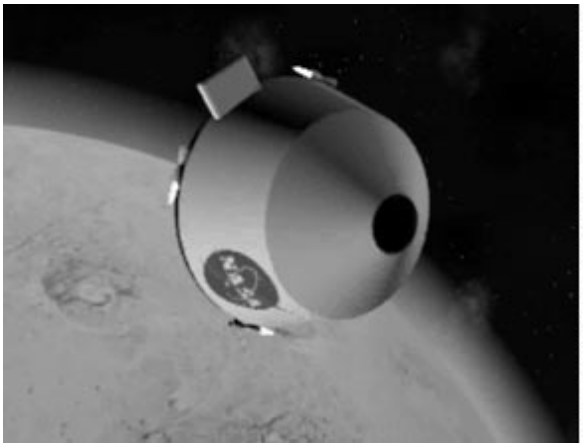

Figure 1. Proposed Mars Smart Lander entry at Mars using flap to provide aerodynamic trim.

It was anticipated that entry of the Mars Surveyor Precision Lander into the atmosphere of Mars (continuum-flow regime) would produce maximum values of normal shock density ratio (ρ_2/ρ_∞) near 20. These high values of normal shock density ratio encountered in hypervelocity flight are produced from

dissociation of atmospheric gases as they cross through the shock wave into the shock layer and are often referred to as real gas effects. It is well recognized that the normal shock density ratio is one of the primary flight simulation parameters that govern the inviscid flow and aerodynamics of blunt bodies at hypersonic speeds[13,14]. Real gas effects can impact the aerodynamics of a vehicle through changes in both the magnitude and distribution of surface pressure. During entry of blunt vehicles into the Martian atmosphere, values of normal shock density ratio are encountered that are significantly larger (2 to 3 times) than those produced in conventional blowdown hypersonic wind tunnels using air or nitrogen as a test gas[13].

Currently active conventional type hypersonic blowdown tunnels are incapable of providing normal shock density ratios near 20. High enthalpy impulse facilities while capable, are not typically utilized from an aerodynamic screening perspective due to extremely short test times. The NASA Langley 20-Inch Mach 6 CF_4 Tunnel was developed to provide a unique alternative to high enthalpy testing[14,15]. This conventional blowdown tunnel utilizes a test gas (tetrafluoromethane-CF_4) with a molecular weight 3 times that of air in order to generate a normal shock density ratio of 12 thereby simulating this particular aspect of a real gas. The simulation is achieved at moderate levels of enthalpy and without dissociation of the test gas. Based upon the proposed entry trajectory of the 2001 Lander, the heavy gas tests in CF_4 simulate a Mach number of approximately 12 based upon a normal shock density ratio of 12 in flight at Mars. An estimate of blunt body aerodynamic effects attributed to a real gas may be obtained by synergistic testing in Mach 6 ideal-air at a comparable Reynolds number.

The Langley 20-Inch Mach 6 Air and CF_4 Tunnels were used to assess the laminar aerodynamic characteristics of the Mars Surveyor 2001 Precision Lander utilizing a flap to provide aerodynamic trim. Three flap sizes were tested at a freestream unit Reynolds number ranging from 0.03 x 10^6/ft to 2.3 x 10^6/ft (post shock Reynolds number based on body diameter of 2,637 to 92,350). The Mars Precision Lander model was tested at angles of attack from 0 deg to 23 deg with select data at 2 deg sideslip. Schlieren images provided details of the shock structure about the proposed entry configuration.

Experimental Methods

Model

The three-inch diameter stainless steel force and moment model is a 0.029 scale representation of the proposed Mars Surveyor 2001 Lander[2]. A dimensioned sketch of the baseline 2001 MSPL flight geometry is shown in Fig. 2. Drawing on the heritage of past planetary missions to Mars, the 2001 Lander forebody consists of a spherically blunted 70-degree half angle cone with a truncated conical afterbody. The model was designed to accept multiple stainless-steel flaps (trim tabs). The flap hingeline was located downstream of the forebody maximum diameter (at the tangency point of the shoulder radius and conical afterbody). At this location, the individual flaps project radially outward, 90 degrees from the longitudinal axis of symmetry.

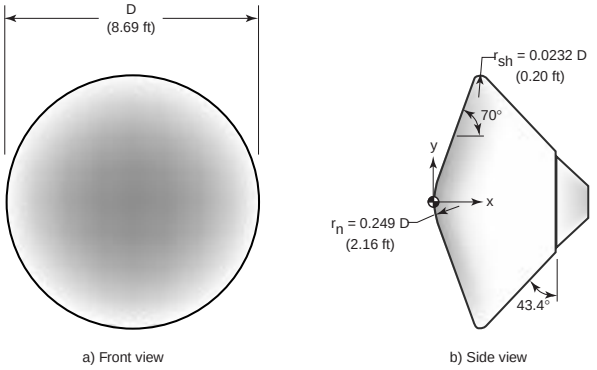

Figure 2. Sketch of 2001 Mars Surveyor Precision Lander Flight Vehicle configuration.

The size of the three candidate flaps examined in this experimental study was initially based on Modified Newtonian predictions as discussed in Ref. 2 and subsequent inviscid computations provided by FELISA (see Computational Methods section). Table 1 details the model/flap configurations that were tested and lists the reference values used to calculate the aerodynamic coefficients. The photographs in Fig. 3 illustrate the flap surface area relative to the forebody frontal area.

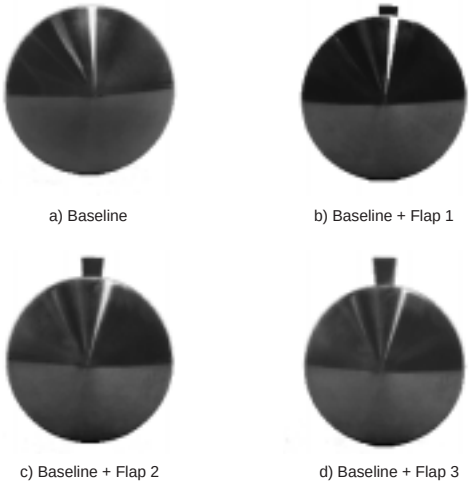

Figure 3. MSPL wind tunnel model with flaps (see table 1).

The projected flap areas normalized to the forebody frontal area are also presented in Table 1.

Facility Descriptions

Tests were conducted in two facilities managed under the Langley Aerothermodynamic Laboratory (LAL). This complex presently consists of four hypersonic wind tunnels that represent a large fraction of the nation's conventional aerothermodynamic test capability[16]. Collectively, they provide a range of Mach number, unit Reynolds number, and normal shock density ratio. This range of hypersonic simulation parameters is due, in part, to the use of two different test gases (air and tetraflouromethane), thereby making the facilities unique national assets. The LAL facilities are relatively small and economical to operate, hence ideally suited for fast-paced aerodynamic performance and aeroheating studies aimed at screening, assessing, optimizing, and bench-marking (when combined with computational fluid dynamics) advanced aerospace vehicle concepts and basic fundamental flow physics research.

20-Inch Mach 6 Air Tunnel: Heated, dried, and filtered air is used as the test gas. Typical calibrated operating conditions for the tunnel are: stagnation pressures ranging from 30 to 500 psia; stagnation temperatures from 410 to 500-degree F; and freestream unit Reynolds numbers from 0.5 to 8 million per foot. A two-dimensional, contoured nozzle is used to provide nominal freestream Mach numbers from 5.8 to 6.1. The closed test section is 20.5 by 20 inches; the nozzle throat is 0.399 by 20.5-inch. A bottom-mounted model injection system can insert models from a sheltered position to the tunnel centerline in less than 0.5-sec. A detailed description of this facility may be found in Ref. 16.

20-Inch Mach 6 CF_4 Tunnel : Heated, dried, and filtered tetrafluoromethane (CF_4) is used as the test gas. Typical calibrated operating conditions for the tunnel are: stagnation pressures ranging from 85 to 2000 psia, stagnation temperatures up to 840-degree F, and freestream unit Reynolds numbers from 0.01 to 0.41 million per foot. A contoured axisymmetric nozzle is used to provide nominal freestream Mach numbers from 5.9 to 6.2. The nozzle exit diameter is 20 inches with the flow exhausting into an open jet test section; the nozzle throat diameter is 0.466-inch. A bottom-mounted model injection system can inject models from a sheltered position to the tunnel centerline in less than 0.5-sec. A detailed description of this facility may be found in Refs. 14 and 15.

Test Conditions and Setup

Nominal reservoir and corresponding free stream flow conditions for the MSPL test series are presented in Table 2. The freestream properties were determined from the measured reservoir pressure and temperature and the measured pitot pressure at the test section. Static pressure in the CF_4 test section that enclosed the open jet were monitored to assess the potential for contraction of the open-jet test core flow with time during any given run. Pitot and reservoir pressures were also measured in both facilities during each run to determine flow conditions and test times. The ratio of projected model frontal area to core flow cross sectional area for the 0.029-scale model is approximately 0.28.

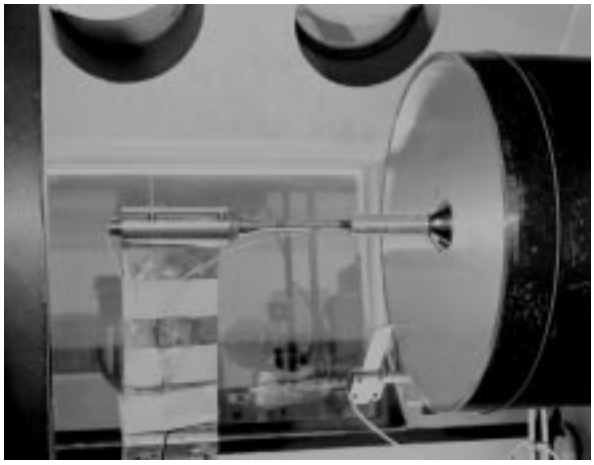

Figure 4. 0.029 scale MSPL aerodynamic model installed in the NASA LaRC 20-Inch Mach 6 CF_4 tunnel.

The model/balance was supported by a cylindrical steel rod (sting) which extended downstream from the model base. In addition, a thin walled protective aluminum shroud extended over the balance and support sting. To determine the possible influence of the support system on aerodynamics, several runs were made with this aluminum shroud removed which decreased the sting-to-forebody diameter ratio (d_s/d_f) from 0.40 to 0.17. Model angle-of-attack and sideslip were set to zero in the tunnel using a combination of an inclinometer and a laser alignment system. A photograph of the MSPL model installation in the CF_4 tunnel is shown in Fig. 4.

Test Techniques

Force and Moment Measurements: Aerodynamic force and moment loads were measured using a sting-supported, six-component, water-cooled internal strain gage balance, Langley-designation HN08B. The balance temperature was monitored using integrated water jacket thermocouples to ensure excessive thermal gradients did not develop during the run. An aluminum shroud was extended over the balance (see Fig. 5) to minimize heating to the balance from base flow impingement. The shroud attached to the sting and clearance was provided to avoid interference with the balance during model movement when aerodynamic forces were applied. In the CF_4

tunnel, the model was located approximately 0.5-inches downstream of the nozzle exit and laterally displaced 4-inches from the tunnel centerline to avoid small disturbances that are characteristic in axisymmetric nozzles. Limited tests made with the model on tunnel centerline did not indicate any measurable effect on the aerodynamic characteristics of the MSPL.

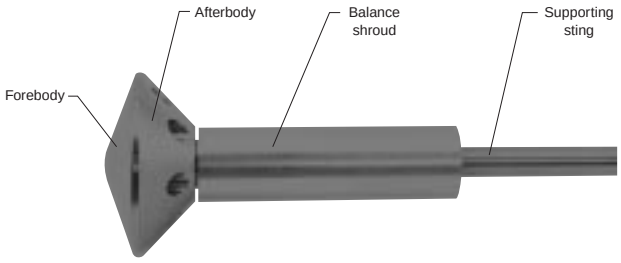

Figure 5. MSPL aerodynamic model with balance shroud.

Schlieren photography: Flow visualization in the form of schlieren was used to complement the surface temperature and heating measurements. The LaRC 20-Inch Mach 6 Air and CF_4 Tunnels are equipped with a pulsed white-light, Z-pattern, single-pass schlieren system with a field of view encompassing the entire test core. The light sources are pulsed for approximately 3 ms. Images were recorded on a high-resolution digital camera and enhanced with commercial software.

Base Pressure Measurements: Base pressure measurements were not obtained during the testing due to the combination of short run times and long base pressure settling times. Previous experience in the CF_4 facility whereby runs were performed at a fixed angle of attack have indicated that rather large diameter tubing is required to insure that base pressure settling times are shorter than the available run time (20 sec). Base pressure measurements with the required tube diameter were not attempted so as to minimize the potential for additional interference effects that may be present due to the balance shroud. As a result, all axial force coefficients, C_A, are reported as uncorrected for base pressure.

Data Reduction and Uncertainty

A 16-bit analog-to-digital facility acquisition system was used to acquire flow condition data. Measured values of $P_{t,1}$ and $T_{t,1}$ are estimated to be accurate to within –2 percent.

Aerodynamic data was obtained in an ascending pitch pause manner during each run. Generally, two separate runs were required to complete a polar due to the short run time. The data was collected by an analog-to-digital data acquisition system using an acquisition rate of 50 samples per second and averaged over a one second interval for each angle of attack (model held at fixed angle of attack for approximately 5 sec). The raw data was transferred to a Hewlett-Packard 9000 computer for data reduction and storage. During data reduction, corrections for weight tares, sting deflections, and balance interactions were made.

The force and moment data measured at the balance electrical center has been transferred to a moment reference center located at the forebody nose along the model x-axis (see Fig. 2). The model outer mold lines were checked and transfer distances were inferred from measurement by the NASA LaRC surface verification laboratory. The balance electrical center was located 2.158 inches behind the configuration moment reference center. Table 1 lists the reference area and lengths used to calculate the aerodynamic coefficients.

Run-to-run repeatability (not shown) of the measured aerodynamic coefficients was generally better than 2%. The estimated uncertainty in the reported coefficients shown in Table 3 is based on 0.5% of the balance full scale load for each component. Based on previous tests, this is considered a conservative estimate and generally will cover uncertainties due to balance accuracy, data acquisition accuracy, transfer distance measurement, and sting deflection.

Computational Methods

An unstructured inviscid flow solver (FELISA[17,18]) was used to provide a rapid assessment of the MSPL aerodynamics. The Langley Aerothermodynamic Upwind Relaxation Algorithm (LAURA)[19,20] was used to provide viscous laminar Navier-Stokes simulations of the MSPL aerodynamics at wind tunnel conditions. Viscous (LAURA) and inviscid (FELISA) computations were made without an afterbody. The same thermodynamic properties for CF_4 were used in both codes. Limited Navier-Stokes predictions were made with the afterbody included to assess the influence of the base on the MSPL aerodynamics.

FELISA

The inviscid flow computations were performed using the unstructured grid software FELISA. This software package consists of a set of computer codes for unstructured grid generation[17], and the simulation of three-dimensional steady inviscid hypersonic flows[18] using unstructured tetrahedral grids. Surface triangulation and discretization of the computational domain using tetrahedral elements is accomplished with two separate codes. The grid used for the baseline MSPL configuration had 43,284 surface points and 902,024 interior points. The hypersonic flow solver

has options for perfect gas air, equilibrium air, CF_4, CO_2, and equilibrium Mars gases. The hypersonic flow solver with the CF_4 gas option was used for the present computations. Flow solutions were computed on a parallel computer. Surface pressures were integrated once every 50 steps during the iterations and the aerodynamic loads were computed. The flow solution was assumed to have converged when these loads reached steady values. The contributions of the base to the aerodynamic loads were ignored (base pressure assumed to be equal to the freestream static pressure.) More information on FELISA software may be found in Ref.17. A description of the hypersonic flow solver may be found in Ref. 18.

LAURA

Computations were performed using the LAURA code. The LAURA code is a three-dimensional, finite-volume solver which includes perfect-gas, equilibrium and non-equilibrium chemistry models, and can be used to solve the inviscid, thin-layer Navier-Stokes, or full Navier-Stokes equations. For the current study, the thin-layer Navier-Stokes equations were solved using the CF_4 gas option. Freestream conditions for the LAURA wind tunnel computations were set to the freestream operating conditions of the test and no-slip conditions were applied at the model wall. A single-block, singularity-free grid topology was employed. The majority of solutions were computed on a forebody- only grid containing -37 x 40 x 32 cells (in the streamwise, circumferential, and body-normal directions, respectively) that included the forward face of the flap. Limited computations were made with an afterbody included to assess the influence of the base on the MSPL aerodynamics. For all solutions, grid adaptation was performed to align the bow-shock with the grid and produced nominal wall cell Reynolds numbers on the order of 1.

A grid resolution study was performed for the configuration with the largest flap. First, the density of the cells in the normal direction was increased beyond the 32 cells in the standard grid. Three solutions were computed for 48, 64, and 96 cells, respectively. Additionally, three solutions for the largest flap were computed on a grid with a much finer surface mesh (148 x 112 cells) for 32, 64, and 96 cells, respectively, in the normal direction.

Results and Discussion

From an experimental viewpoint, the MSPL aerodynamic flap feasibility study conducted in the M_∞=6 CF_4 tunnel was initially desirable from the perspective of testing in a gas with a high normal shock density ratio and a corresponding low ratio of specific heats (γ) - as is encountered in hypervelocity flight. In addition, the facility provides the best opportunity from which to maintain a laminar flow since it operates at relatively low Reynolds numbers. More importantly, the Shuttle Orbiter first flight experience has underscored the importance of quantifying real gas effects. As detailed in Ref. 21, the Shuttle experienced a significant nose-up pitching moment increment relative to pre-flight predictions resulting in body flap deflections of twice the amount necessary to achieve trimmed flight. This phenomenon was later accurately simulated in the Langley CF_4 tunnel and was coupled with computational methods to provide a high degree of confidence in estimating hypersonic entry aerodynamics[21]. It is commonly recognized today that the primary effect of a real gas on aerodynamics is to lower the specific heat ratio (γ) within the shock layer which in turn will produce a greater degree of flow compression and expansion relative to a perfect gas. Thus, compression surfaces (such as flaps) will have a correspondingly higher surface pressure. Because of the presence of a control surface near the rapidly expanding flow near the MSPL shoulder, aerodynamic real gas simulation testing (similar to that conducted on the Viking Lander and Shuttle Orbiter post-flight) were performed.

From a computational aerodynamic screening perspective, FELISA provided a rapid assessment of the viability of a flap to provide aerodynamic trim. For the MSPL, a target L/D of at least 0.18 was required to provide adequate margins for a precision landing and was preferred based on Viking flight experience. I Aerodynamic predictions at wind tunnel conditions provided by FELISA, Fig. 6a-b, indicated that a properly sized flap could provide sufficient aerodynamic trim at the required L/D.

The inviscid results from FELISA would not capture viscous effects such as skin friction and/or flow separation. Since skin friction over a forebody such as the MSPL for hypersonic freestream conditions at sufficiently high Reynolds number is negligible and afterbody contributions to aero are minimal, inviscid prediction should capture the overall aerodynamics (provided viscous effects on the MSPL flap are minimal).

Performance of the three flaps from the experimental heavy gas simulation tests relative to the measured baseline longitudinal aerodynamics (C_A, C_m, C_N, and L/D) of the MSPL at M_∞=6 CF_4, $\rho_2/\rho_\infty = 12$, and Re_{2D}=0.03 x 10^6 are summarized in Fig. 7a-d. Since the baseline shape is axisymmetric (with no flap), it trims at $\alpha = 0$ degrees with an L/D =

0. As anticipated, the primary effect of the flaps was to change the MSPL trim angle of attack. At wind tunnel conditions, a flap surface area approximately 6 percent of the forebody frontal area (Flap 3) was shown to trim the MSPL near α=11.5 degrees (Fig. 7b) at the desired L/D value of 0.18 (Fig. 7d). In comparison, Viking flight experience indicated the lander trimmed near 11 degrees angle of attack (via a c.g. offset) during its entry at Mars[22].

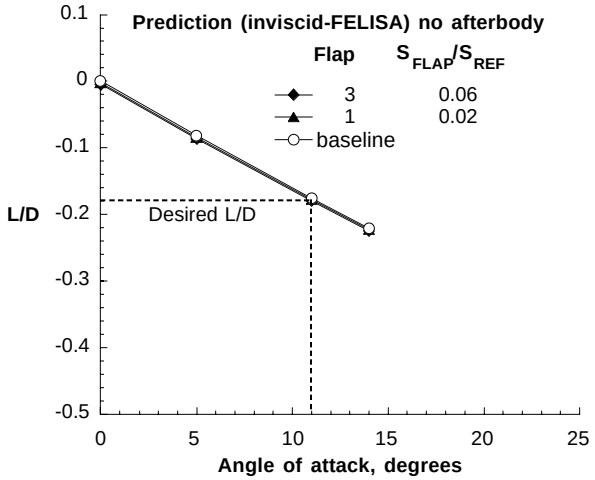

a) lift-to-drag ratio

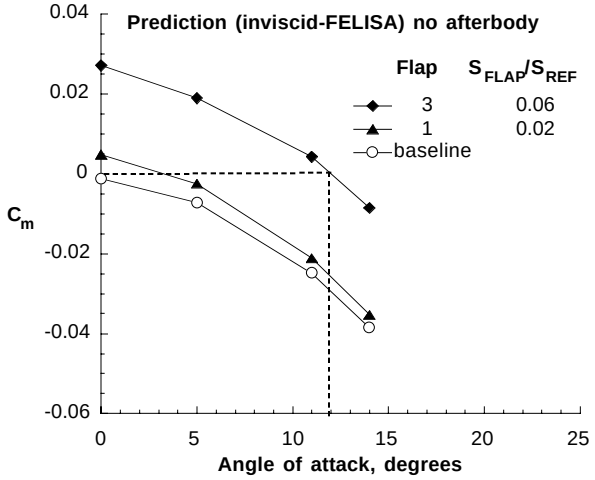

b) pitching moment coefficient

Figure 6. Inviscid prediction of MSPL longitudinal aerodynamics provided by FELISA. M_∞=6, CF_4, Re_{2D}=0.03 x 10^6, ρ_2/ρ_∞=11.7.

The addition of the flaps on the MSPL was found to have no measurable effect on L/D performance (since L and D derived primarily from C_A), but did produce measurable increases in axial force (Fig. 7a).

The effect of normal shock density ratio on laminar MSPL pitching moment coefficient measurements obtained with the baseline and the baseline with the largest flap (flap 3) in air and CF_4 at identical Mach and Reynolds numbers, are shown in Fig. 8a-b. The pitching moment measurements made with the largest flap, Fig. 8b suggest favorable real gas effects at trim conditions; MSPL heavy gas simulation tests indicated a trimmed condition at 11.5 degrees in contrast to 8.5 degrees measured in air. The data indicate greater pitching moment stability (more negative slope) than measured in air for α > 10 degrees. The corresponding laminar MSPL baseline (no flap-Fig. 8a) measurements obtained in air and CF_4 at identical Mach and Reynolds numbers, exhibited the same stabilizing effect in CF_4 on pitching moment and were consistent with ground based trends measured for Viking[23]. The cross over in pitching moment between the present air and CF_4 tests are consistent with Viking test experience.

No attempt was made in this screening study to optimize flap trim effectiveness through flap shape, orientation, or attachment location parametrics. In the context of the more mature MSPL designs, the flap was considered to be deployable retrofit as packaging a fixed control surface within the diameter of the launch vehicle shroud was unlikely. In the conceptual stages of this study, it was felt that the most effective location for the flap would be at or near the vehicle shoulder where the moment arm for the flap pressure loading is greatest. The deployable flap hingeline was located downstream of the forebody maximum diameter in a potentially more benign heating environment. In this position, the shadowed region in front of the flap was expected to produce a local flow separation[2]. Subsequent flow reattachment on the flap would result in an embedded shock. If a fixed flap was permissible, a simple surface extension beyond the conical forebody, such as that investigated in Ref. 12, might prove beneficial. This would eliminate the embedded shock system thereby minimizing flap effectiveness sensitivity to Mach number, Reynolds number, and density ratio and avoid heating increases (see Ref. 24) due to flow reattachment on the flap. These benefits would be weighted against the reduced flap pressure loading (and resultant requirement to increase flap size) in the absence of an embedded shock system.

Figs. 9-12 show the comparisons of the measured longitudinal aerodynamics (C_A, C_m, C_N, and L/D) of the MSPL at M_∞=6 CF_4, ρ_2/ρ_∞ = 12, and Re_{2D}=0.03 x 10^6 to viscous predictions from LAURA at α = 0 and 11 degrees. Even with the afterbody excluded from the computations, the predicted pitching moment and normal force coefficients from LAURA were within the uncertainty of the measurement. Axial force coefficient

prediction was generally 1 to 4% lower than measurement and thus generally outside the lower limit of the estimated uncertainty. A grid resolution study was performed on the baseline configuration with flap 3. An increase in wall normal cells from 32 to 96 produced a small increase (0.7%) in the axial aerodynamic coefficient, Fig. 12a. The corresponding comparisons of predicted pitching moment and normal force coefficients for this grid resolution study, Fig. 12b-c were virtually indistinguishable. For aerodynamic screening purposes, this suggested that the impact of the embedded shock near the flap was adequately resolved with 32 cells in the normal direction.

The influence of the base on MSPL hypersonic aerodynamics was expected to be minimal. Previous blunt body testing[25] in the CF_4 tunnel with an afterbody attached and removed had indicated no measurable effect on longitudinal aerodynamics. Computational predictions made with LAURA on the MSPL baseline configuration with and without an afterbody are shown in Fig. 13. At $\alpha = 0$ degrees, the presence of an afterbody increased C_A by approximately 0.02 and brought the difference between the predicted axial force coefficient and measurement to less than 1%. Comparing the magnitude of the computed base pressure correction (by including the afterbody)to those estimated from an engineering formula,[26]

$$\Delta C_{A,\ base\ correction} = (1/M_\infty{}^2) - (0.57/M_\infty{}^4) \quad (1)$$

indicated the LAURA corrections (with/without afterbody) to be 25% smaller. The increment in C_A and the differences in the magnitude of the correction with and without an afterbody are consistent with previous hypersonic LAURA blunt body analysis.[27] and indicated a viscous shear contribution from the afterbody. The corresponding comparisons of predicted pitching moment and normal force coefficients in the presence and absence of an afterbody show the results are virtually indistinguishable.

It is also generally recognized that the presence of a support sting may have an effect on the base flow characteristics of a blunt body in hypersonic flow. Experimental quantification of the effect with and without a support sting for this test series was not made. However, a limited data set was taken to assess the sensitivity of the MSPL aerodynamic drag measurements to the potential effects of a cylindrical model support sting for sting-to-model forebody diameter ratios of 0.40 (balance shroud attached - see Fig. 5) and 0.17 (balance shroud removed). At Re_{2D}=0.03 x 10^6, M_∞=6 CF_4, and α=0 degrees, no measurable aerodynamic effect from the differences in model support was observed (not shown). Measurements at incidence were not attempted as flow impingement on the unprotected balance (shroud removed) was anticipated.

As the MSPL baseline configuration was symmetric, it was anticipated that the vehicle would be laterally/directionally stable at sideslip angles anticipated for flight (β < 2 degrees). The lateral/directional characteristics of the MSPL with a flap were not known. A limited assessment of static lateral/directional aerodynamics ($C_{y,\beta}$, $C_{l,\beta}$, and $C_{n,\beta}$) of the MSPL (configured with flap 3) at a side slip angle of 2 degrees, indicated the lander was stable as shown in Fig. 14 through the test range of angle of attack.

Schlieren images for the MSPL baseline and baseline plus flaps (at M_∞=6 CF_4, Re_{2D}=0.03 x 10^6) are presented in Fig. 15, for α=11 degrees. In the sequence of images, an embedded shock associated with the flow expansion and separation around the aerobrake shoulder, and subsequent reattachment and recompression is evident for all three flaps. The flap aerodynamic effectiveness in flight would be dictated by the strength of this embedded shock. Further quantification of real gas effects and Mach number on flap pressure loading would be essential in determining the viability of any flap to provide aerodynamic trim at the appropriate values of L/D for the duration of its atmospheric trajectory.

Schlieren images for the MSPL baselione plus flap 3 (in M_∞=6 CF_4, Re_{2D}=0.03 x 10^6) are presented in Fig. 16, for a range of angle of attack ($0<\alpha<+20$ degrees). As expected, the embedded shock system persists over the range of angle of attack. Comparison of the measured shock shape of the MSPL baseline + flap 3 at α = 11 degrees with thin layer Navier Stokes prediction (for the 148 x 112 x 96 grid) are presented in Fig. 17. The predicted bow shock standoff distance and the spatial location and shape of the embedded shock associated with the flap (inferred from the computational density contour mapping) was in excellent agreement (within 2%) with measurement.

Concluding Remarks

The Langley 20-Inch Mach 6 Air and CF_4 Tunnels were used to assess the aerodynamic characteristics of the Mars Surveyor 2001 Precision Lander utilizing a base flap to provide aerodynamic trim. Three flap sizes were evaluated over a range of freestream unit Reynolds number from 0.03 x 10^6 to 2.23 x 10^6 at a nominal free stream Mach number of 6. The model was tested at angles of attack from 0¡ up to 23¡ with select data at 2¡ sideslip. Based upon the proposed entry trajectory of the MSPL, the heavy gas

tests in CF_4 simulate a Mach number of approximately 12 based upon a normal shock density ratio of 12 in flight at Mars. The resulting laminar aerodynamic measurements obtained in air and CF_4 at comparable Mach and Reynolds number, indicate favorable real gas effects at trim conditions. The CF_4 data indicate greater pitching moment stability than measured in air for $\alpha >$ 10 degrees; MSPL heavy gas simulation tests with the largest flap indicated a trimmed condition at 11.5 degrees angle of attack in contrast to 8.5 degrees measured in perfect gas air. A limited assessment of static lateral/directional aerodynamics at a side slip angle of 2 degrees indicated the lander was stable through the test range of angle of attack.

Inviscid prediction with an unstructured hypersonic flow solver (FELISA) provided a rapid assessment on the viability of a flap to provide aerodynamic trim at the desired L/D. Longitudinal aerodynamic coefficients predicted with a viscous solver (LAURA) were generally within the estimated measurement uncertainty. Computations which included the afterbody brought the difference between the predicted axial force coefficient and measurement to less than 1%.

When traditional means of providing aerodynamic trim for this blunt class of planetary entry vehicle are not possible (offset c.g.), a single flap can provide similar aerodynamic performance. Whether fixed or deployable, the viability of the flap to a provide trim capability would reside in trade studies to determine mass/ballast penalties associated with flap attachment or deployment hardware and additional control surface thermal protection requirements.

Acknowledgments

Without the assistance of the following individuals this work would not have been possible: Ed Carden, Harry Stotler, Mike Fleck, Dave Fahringer, Dave Roberts, Alan Scheidegger, Ed Covington and Tom Burns for model design/ fabrication/ instrumentation/ surface inspection support; Grace Gleason, John Ellis, Roland Hatten, Melanie Lawhorne, Harry Stotler, Christal Kellam, and Al Garner for wind tunnel support; Sheila Wright and Bert Senter for data acquisition assistance, Robert Braun, Robert Mitcheltree, and Ken Sutton for technical discussions; and Richard Wheless for documentation assistance. The authors gratefully acknowledge their contributions and behind-the- scenes work.

References

1. Lockwood, M. K., Powell, R. W., Graves, C. A., and Carman, G. L., "Entry System Design Considerations for Mars Landers," AAS 01-023, January, 2001.

2. Braun, R. D., Powell, R. W., Cheatwood, F. M., Spencer, D. A., and Mase, R. A., "The Mars Surveyor 2001 Lander: A First Step Towards Precision Landing," IAF-98-Q.3.03, 1998.

3. Smith, B. A., "Lander Development Paced By Mars Science Results," *Aviation Week & Space Technology*, June. 26, 2000, p. 63.

4. Pieri, D., "Rebuilding the U.S. Mars Exploration Program," *Launchspace*, July/Aug., 2000, p. 27.

5. Smith, B. A., "NASA Weighs Mission Options," *Aviation Week & Space Technology*, Dec. 11, 2000, p.54.

6. Lockwood, M. K., Sutton, K., Prabhu, R., Powell, R., Graves, C., and Epp, C., "Entry Configurations and Performance Comparisons for Mars Smart Lander," AIAA 2002-4407, August, 2002.

7. Striepe, S. A., Queen, E. M., Powell, R. W., Aguirre, J. T., Sachi, L. A., and Lyons, D. T., "An Atmospheric Guidance Algorithm Testbed for the Mars Surveyor Program 2001 Orbiter and Lander," AIAA-98-4569, August, 1998.

8. Carman, G., Ives, D., and Geller, D., "Apollo-Derived Mars Precision Lander Guidance," AIAA-98-4570, August, 1998.

9. Tu, K.-Y., Munir, M., Mease, K., and Bayard, D., "Drag-Based Predictive Tracking Guidance for Mars Precision Landing," AIAA-98-4573, August, 1998.

10. Powell, R. W., "Numerical Roll Reversal Predictor-Corrector Aerocapture and Precision Landing Guidance Algorithms for the Mars Surveyor Program 2001 Missions," AIAA-98-4574, August, 1998.

11. Blanchard, R. C., Wilmoth, R. G., and Moss, J. N., "Aerodynamic Flight Measurements and Rarefied-Flow Simulations of Mars Entry Vehicles," *J. of Spacecraft and Rockets*, vol. 34, no. 5, p 687-690, 1997.

12. Sammonds, R. I. and Dickey, R. R., "Effectiveness of Several Control Arrangements On A Mercury-Type Capsule," NASA TM X-579, 1961.

13. Jones, R. A. and Hunt, J. L., "Use of Tetrafluoromethane to Simulate Real-Gas Effects on the Hypersonic Aerodynamics of Blunt Bodies," NASA TR R-312, 1969.

14. Midden, R. E. and Miller, C. G. III, "Description and Calibration of the Langley Hypersonic CF_4 Tunnel: A Facility for Simulating Low Gamma Flow as Occurs for a Real Gas," NASA TP 2384,

1985.

15. Micol, J. M., Midden, R.E., and Miller, C.G. III, "Langley 20-Inch Hypersonic CF_4 Tunnel: A Facility for Simulating Real Gas Effects," AIAA 92-3939.

16. Miller, C. G. III, "Langley Hypersonic Aerodynamic/Aerothermodynamic Testing Capabilities - Present and Future," AIAA Paper 90-1376, June 1990.

17. Peiro, J., Peraire, J., and Morgan, K., "FELISA System Reference Manual and Users Guide," Tech. Report, University College of Swansea, UK., 1993.

18. Bibb, K. L., Peraire, J., and Riley, C. J., "Hypersonic Flow Computations on Unstructured Meshes," AIAA Paper 97-0625, 1997.

19. Gnoffo, P. A., "An Upwind-Biased, Point-Implicit Relaxation Algorithm for Viscous Compressible Perfect Gas Flows," NASA TP 2953, Feb., 1990.

20. Cheatwood, F. M. and Gnoffo, P. A., "User's Manual for the Langley Aerothermodynamic Upwind Relaxation Algorithm (LAURA)," NASA TM 4674, April, 1996.

21. Brauckmann. G. J., Paulson, J. W. and Weilmuenster, J. K., "Experimental and Computational Analysis of the Space Shuttle Orbiter Hypersonic Pitch-Up Anomaly," AIAA Paper 94-0632, January 1994.

22. Blanchard, R. C., Wilmoth, R. G., and Moss, J. N., "Aerodynamic Flight Measurements and Rarefied-Flow Simulations of Mars Entry Vehicles," *J. of Spacecraft and Rockets*, vol. 34, no. 5, p 687-690, 1997.

23. Hunt, J. L., Jones, R. A., and Midden, R. E., "Simulation of Real-Gas Effects for Mars Entry," *J. of Spacecraft and Rockets*, vol. 11, no. 1, p 62-64, 1974.

24. Liechty. D. S., and Hollis, B. R., "Experimental Control Surface and Afterbody Aeroheating Characteristics for a Proposed Mars Smart Lander," AIAA Paper 2002-4506, August 2002.

25. Wells, W. L., "Measured and Predicted Aerodynamic Coefficients and Shock Shapes for Aeroassist Flight Experiment (AFE) Configuration," NASA TP-2956, Jan., 1990.

26. Bonner, E., Cleaver, W., and Dunn, K., "Aerodynamic Preliminary Analysis System II. Part I-Theory," NASA CR-182076, April, 1991.

27. Wood, W. A., Gnoffo, P. A., and Rault, D. F., "Aerodynamic Anaylis of Commercial Experiment Transporter Re-Entry Capsule," *J. of Spacecraft and Rockets*, vol. 33, no. 5, p 643-646, 1996.

Table 1. Model Configurations

Configuration	L_{ref} (in.)	S_{ref} (in.)	b_{ref} (in.)	$X_{c.g.}$(in.)	$S_{Flap}/S_{Forebody}$
Baseline	3	7.07	3	0	-
Baseline + Flap 1	3	7.07	3	0	0.0212
Baseline + Flap 2	3	7.07	3	0	0.0398
Baseline + Flap 3	3	7.07	3	0	0.0606

Table 2. Nominal flow conditions

Re_∞/ft (x10^6)	$Re_{2,D}$	M_∞	Test gas	$P_{t,1}$(psi)	$T_{t,1}$(¡R)	ρ_2/ρ_∞
0.66	26,425	5.8	air	33	866	5.23
1.23	49,125	5.9	air	64	879	5.24
2.33	92,350	5.9	air	130	900	5.26
0.03	2,637	6.0	CF_4	119	1305	12.0
0.11	10,935	5.8	CF_4	388	1305	11.7
0.32	31,175	5.9	CF_4	1069	1296	11.8

Table 3. Estimated Force & Moment Coefficient Uncertainties

C_N	C_A	C_Y	C_m	C_n	C_l
±.008	±.015	±.004	±.003	±.001	±.001

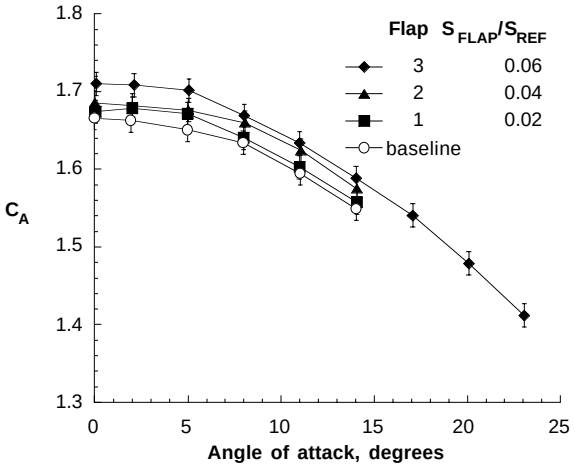

a) axial force coefficient

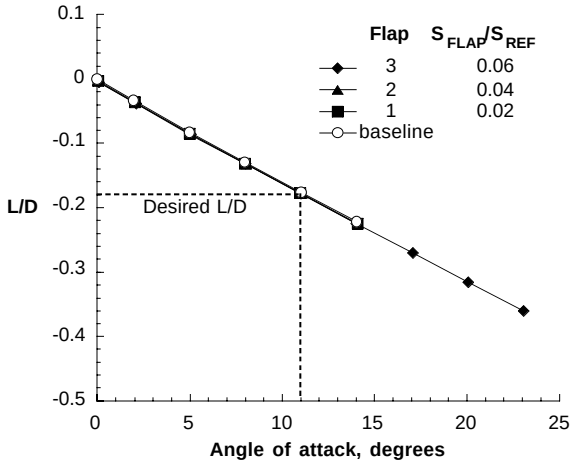

d) lift-to-drag ratio

Figure 7. Effect of flap size on MSPL longitudinal aerodynamics. M_∞=6, CF_4, Re_{2D}=0.03 x 10^6, ρ_2/ρ_∞=11.7.

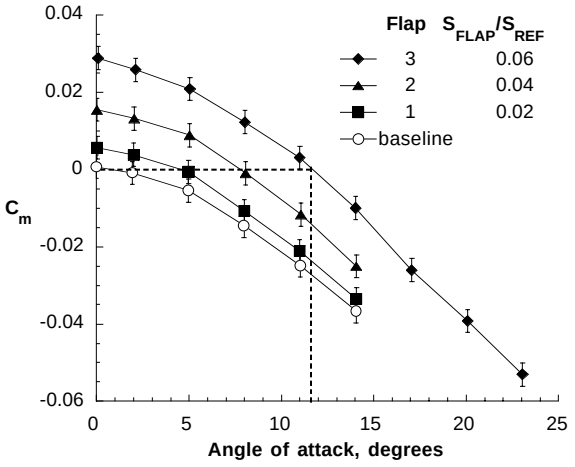

b) pitching moment coefficient

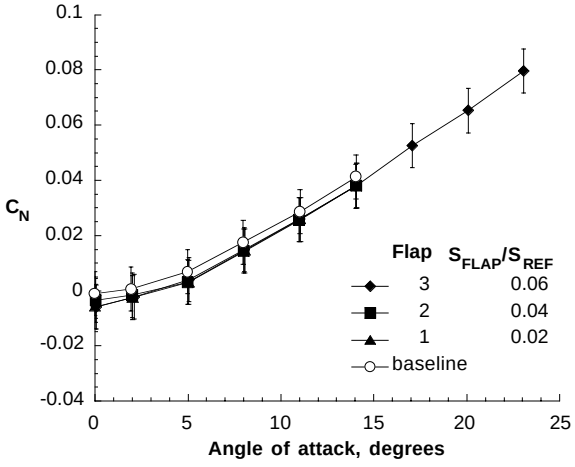

c) normal force coefficient

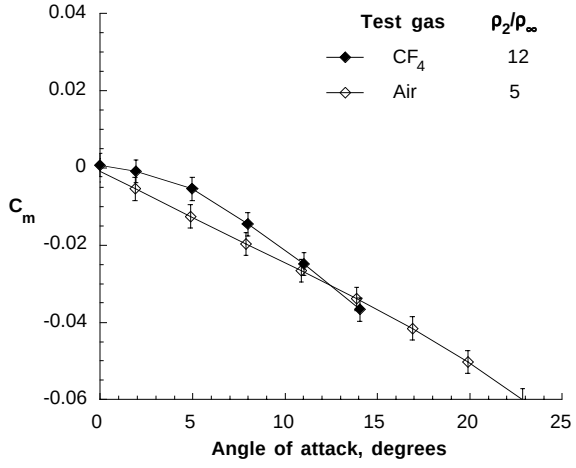

a) baseline

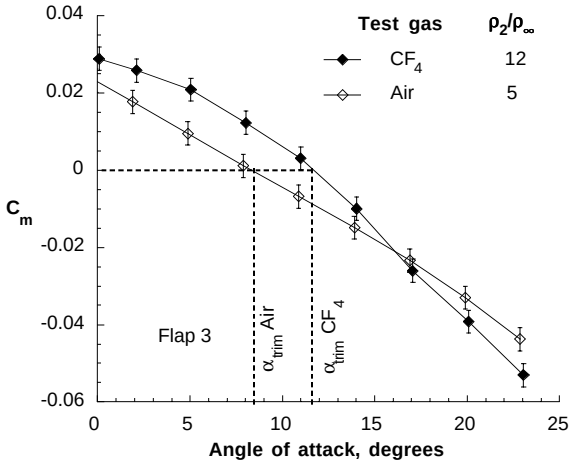

b) baseline + Flap 3

Figure 8. Effect of normal shock density ratio on MSPL pitching moment coefficient. M_∞=6, Re_{2D}=0.03 x 10^6.

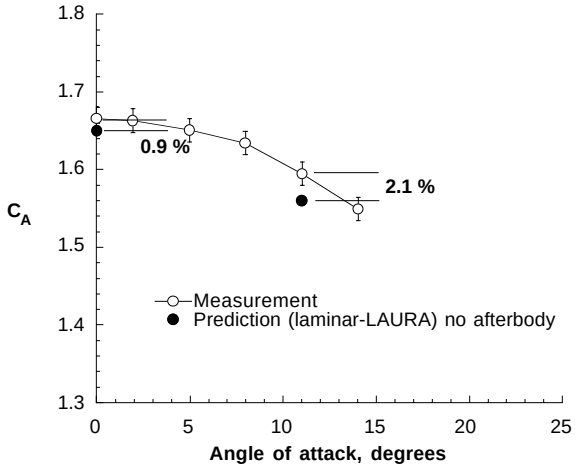

a) axial force coefficient

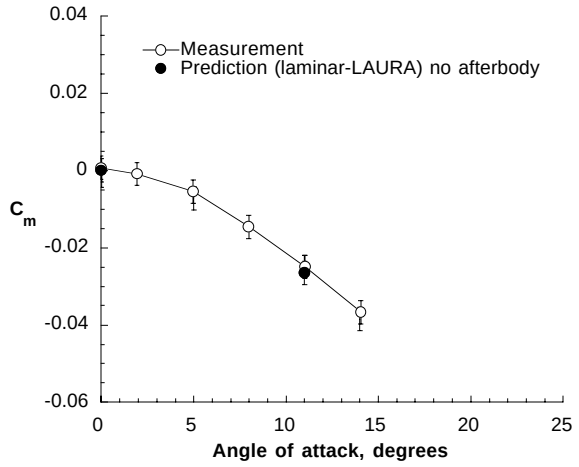

b) pitching moment coefficient

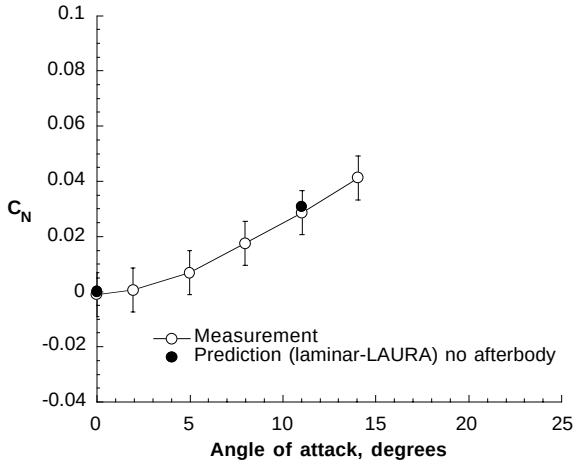

c) normal force coefficient

Figure 9. Comparison of baseline MSPL longitudinal aerodynamics with prediction. M_∞=6, CF_4, Re_{2D}=0.03 x 10^6, ρ_2/ρ_∞=11.7.

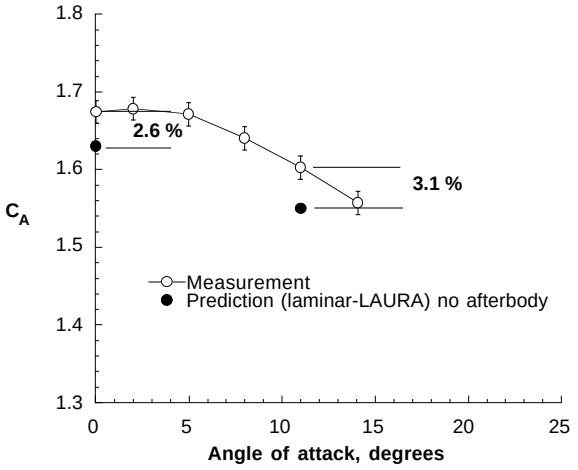

a) axial force coefficient

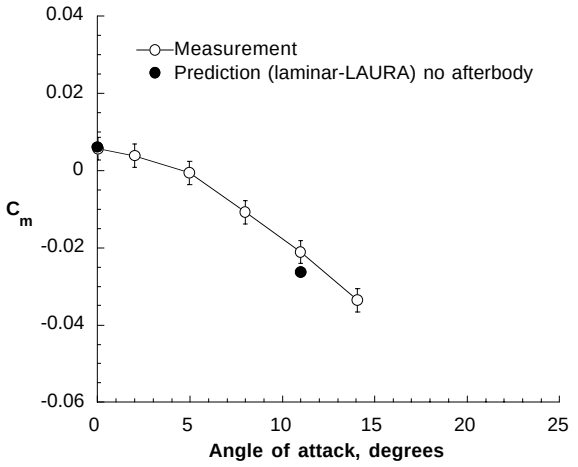

b) pitching moment coefficient

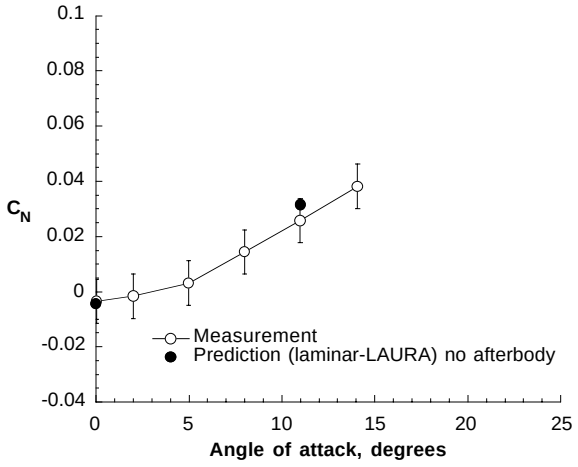

c) normal force coefficient

Figure 10. Comparison of baseline + flap 1 MSPL longitudinal aerodynamics with prediction. M_∞=6, CF_4, Re_{2D}=0.03 x 10^6, ρ_2/ρ_∞=11.7.

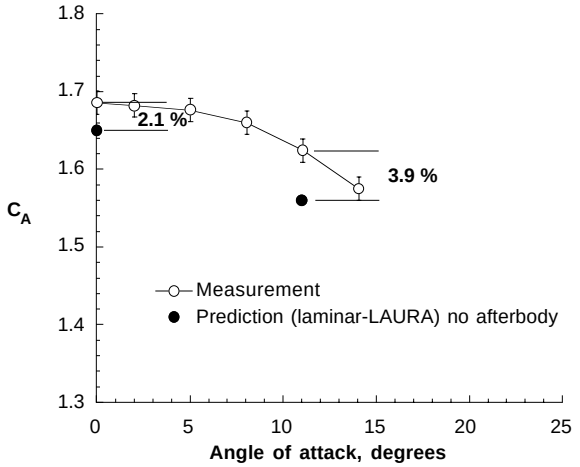

a) axial force coefficient

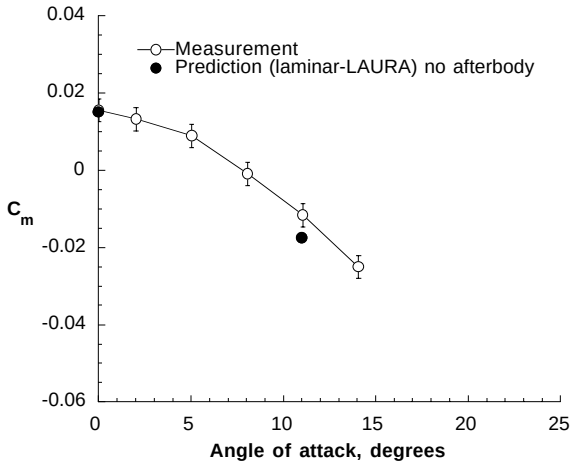

b) pitching moment coefficient

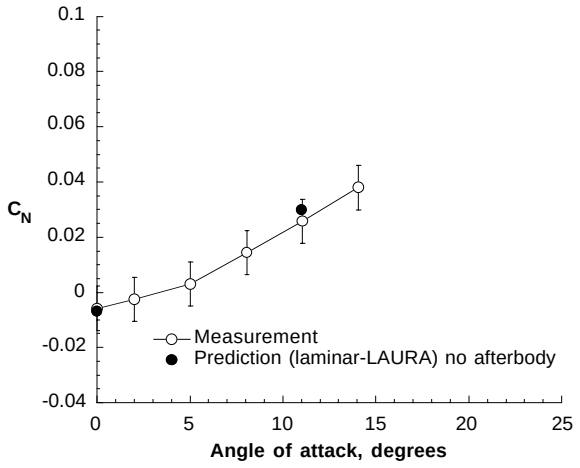

c) normal force coefficient

Figure 11. Comparison of baseline + flap 2 MSPL longitudinal aerodynamics with prediction. M_∞=6, CF_4, Re_{2D}=0.03 x 10^6, ρ_2/ρ_∞=11.7.

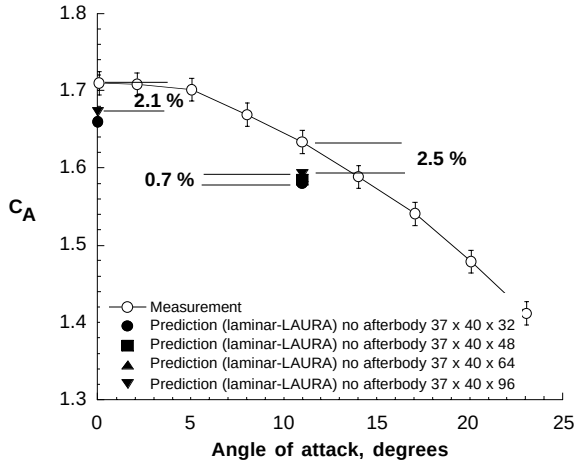

a) axial force coefficient

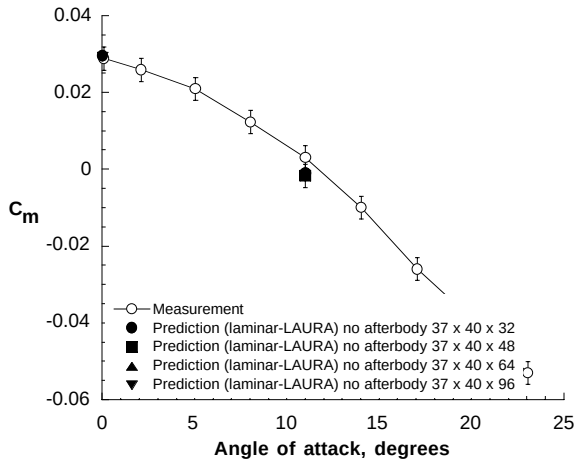

b) pitching moment coefficient

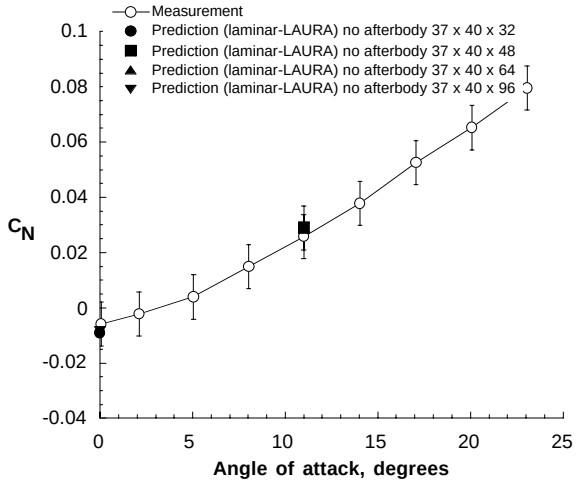

c) normal force coefficient

Figure 12. Comparison of baseline + flap 3 MSPL longitudinal aerodynamics with prediction. M_∞=6, CF_4, Re_{2D}=0.03 x 10^6, ρ_2/ρ_∞=11.7.

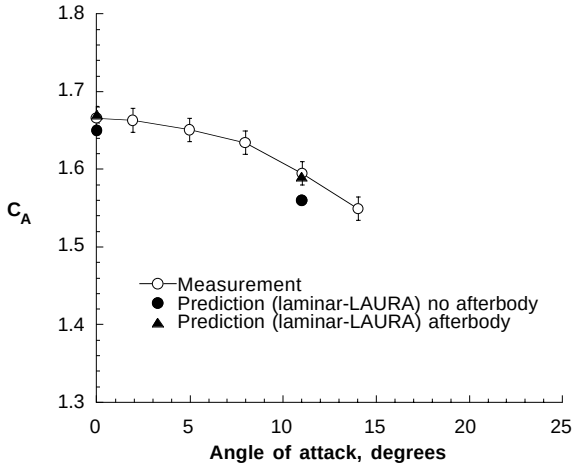

a) axial force coefficient

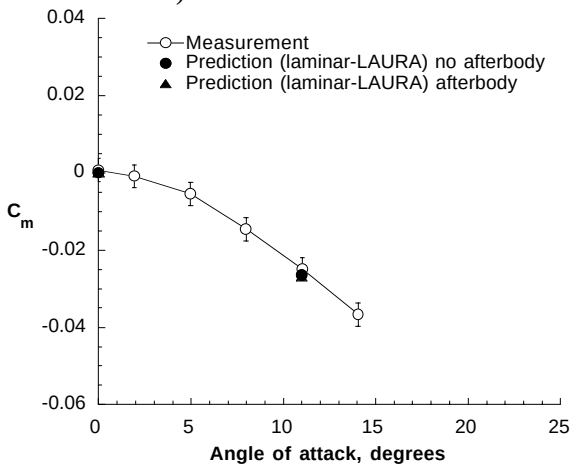

b) pitching moment coefficient

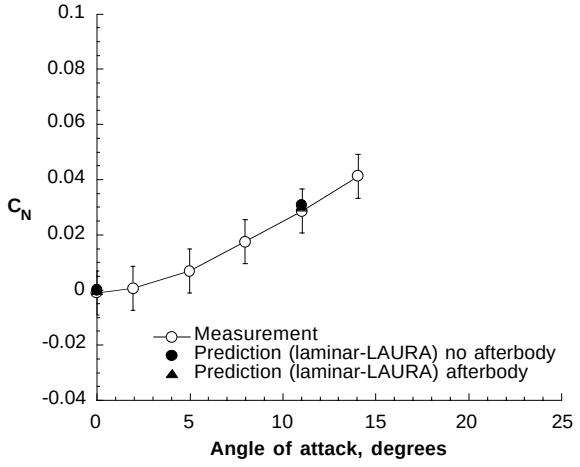

c) normal force coefficient

Figure 13. Effect of afterbody on predicted baseline MSPL longitudinal aerodynamics and comparison to measurement. M_∞=6, CF_4, Re_{2D}=0.03 x 10^6, ρ_2/ρ_∞=11.7.

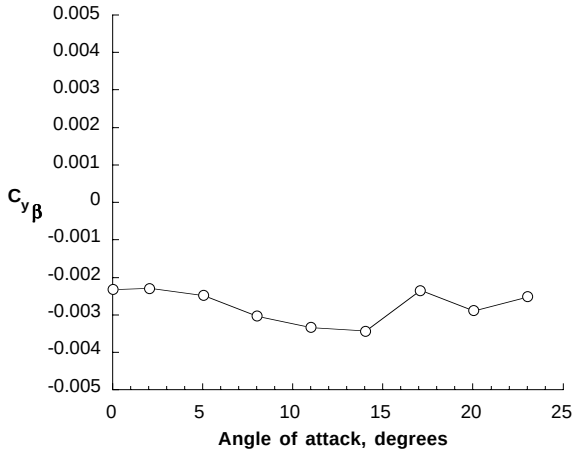

a) side force derivative

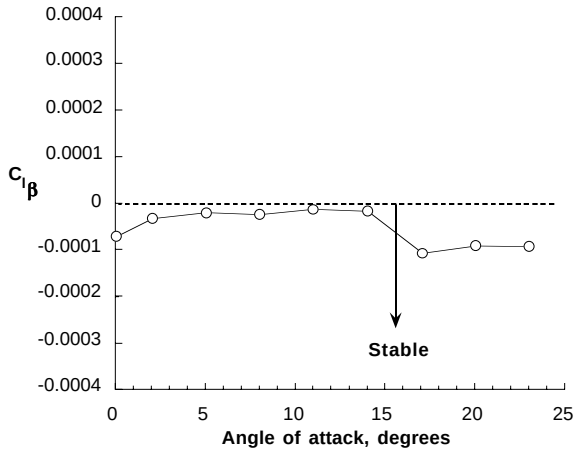

b) rolling moment derivative

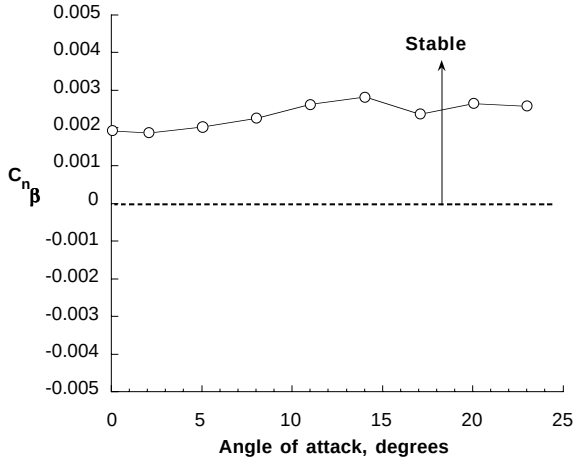

c) yawing moment derivative

Figure 14. MSPL lateral/directional aerodynamics. M_∞=6, CF_4, Re_{2D}=0.03 x 10^6, ρ_2/ρ_∞=11.7, β = –2 degrees.

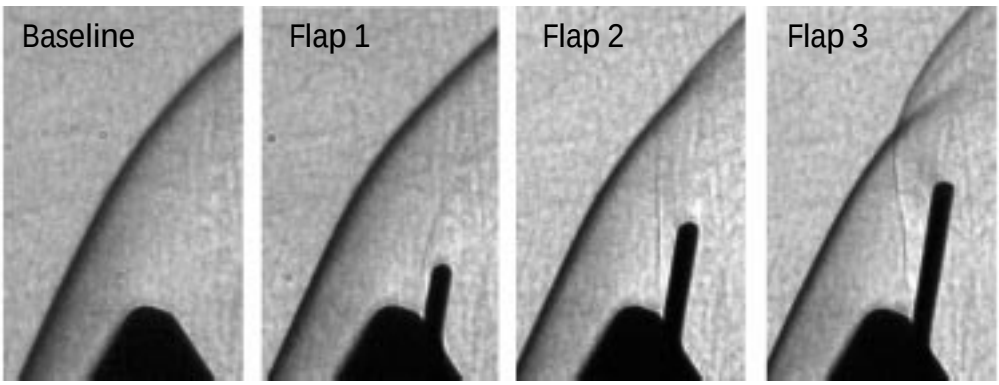

Figure 15. Effect of flap size on MSPL shock shape and interaction. M_∞=6, CF_4, ρ_2/ρ_∞=11.7, Re_{2D}=0.03 x 10^6, α= 11 degrees.

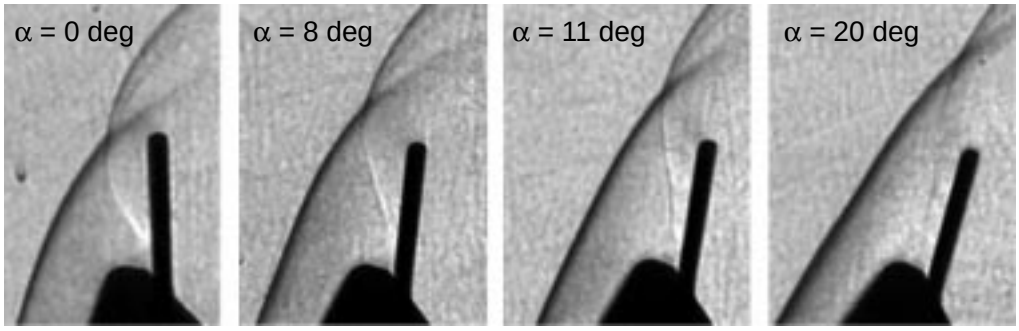

Figure 16. Effect of angle of attack on MSPL shock shape and interaction. M_∞=6, CF_4, ρ_2/ρ_∞=11.7, Re_{2D}=0.03 x 10^6, flap 3.

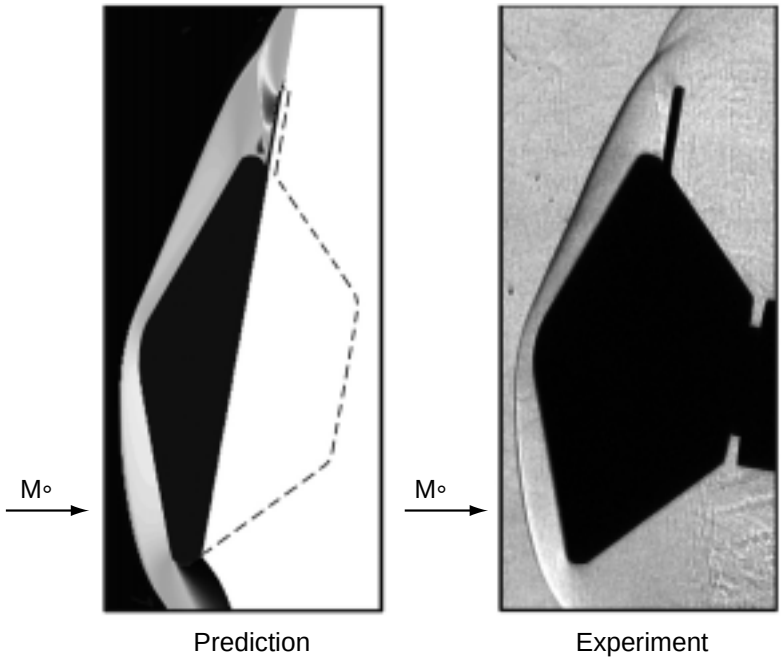

Figure 17. Comparison of predicted MSPL density contours with measured schlieren image. M_∞=6, CF_4, ρ_2/ρ_∞=11.7, Re_{2D}=0.03 x 10^6, α= 11 degrees, flap 3.